

Structural Commonalities in Different Classes of Non-Crystalline Materials

I. Rodríguez¹, D. Hinojosa-Romero², R. M. Valladares², A. Valladares², A. A. Valladares^{1*}

1. Instituto de Investigaciones en Materiales, Universidad Nacional Autónoma de México, Apartado Postal 70-360, Ciudad Universitaria, CDMX, México City 04510, México.

2. Facultad de Ciencias, Universidad Nacional Autónoma de México, Apartado Postal 70-542, Ciudad Universitaria, CDMX, México City 04510, México.

*Corresponding author: Ariel A. Valladares, valladar@unam.mx

ABSTRACT

In the past decades, the research community has explored diverse structures and new fabrication methods of non-crystalline solids. Glassy materials that belong to the semiconductor realm and to the metallic type are the most studied both experimentally and theoretically. The present work investigates similar structural trends whenever they exist and different trends among different classes. Amorphous semiconductors display Pair Distribution Functions (PDF) that are very similar among themselves, and this indicates that these network-forming materials have properties that are alike. Analogously, metallic systems have comparable PDFs but different from the network forming materials, as it should be, since the properties between these two classes are quite different. Here we pay attention to the first and second peaks of their structures. Whereas the semiconductor structures display a simple first and second peak with a near-zero value between them. In contrast, the metallic systems have a very well-defined non-zero value between the first and second peaks, and they also display what we have come to identify as an “elephant peak”. We also discuss semimetals and alloys.

INTRODUCTION

The atomic-scale structure of a material governs its properties, establishing the cornerstone of modern materials science. While crystalline solids benefit from well-established structure-property relationships enabled by long-range order, non-crystalline materials, such as glasses, amorphous metals, and liquids, present a formidable challenge due to their inherently disordered atomic arrangements. Despite their technological importance in applications ranging from semiconductors to metallic glasses, the absence of translational symmetry in these materials has long hindered a unified understanding of their structural organization. Recent advances in local-structure characterization techniques, particularly pair distribution function (PDF) and plane-angle distribution (PAD), have emerged as a powerful lens to decode the short-range and medium-range order that defines these systems.

Over the past two decades, our research group has systematically investigated the atomic structure of diverse non-crystalline materials, beginning with covalent semiconductors such as amorphous silicon and carbon [1], and expanding to include metallic glasses (e.g., Al [2], Pd [3], Bi [4]), alloys (Cu-Zr [5], Au-Ag [6]) and liquids [Andres, Flor]. This extensive dataset, accumulated through synchrotron X-ray scattering and *ab initio* molecular dynamics simulations (AIMD), has revealed intriguing structural patterns that transcend individual material classes. Notably, PDFs—which quantify the probability of atomic pair distances—exhibit class-specific signatures in their first and second coordination shells. For instance, covalent amorphous solids display pronounced first-peak splitting linked to bond-angle distortions, while metallic glasses show asymmetric second peaks indicative of medium-range packing motifs. These features correlate strongly with macroscopic behaviors such as mechanical stability, glass-forming ability, and electronic properties.

Despite these advances, a systematic exploration of structural commonalities across distinct classes of non-crystalline solids remains lacking. Do universal principles underlie the diversity of disordered structures? Can subtle similarities in PDF peak shapes or coordination statistics inform predictive models for new materials? This study addresses these questions by conducting a comparative PDF and PAD analysis of covalent, metallic, and alloy-based amorphous systems. By identifying shared structural motifs—such as distorted polyhedral units or percolative medium-range clusters—we establish a framework to classify non-crystalline materials based on their local order. Our findings deepen the understanding of disorder-property relationships and pave the way for designing amorphous materials with tailored functionalities.

METHOD

The *undermelt-quench* method constitutes a computational protocol specifically devised to generate physically realistic amorphous structures. This technique systematically destabilizes a crystalline precursor, subsequently kinetically arresting the system into a disordered configuration. This approach is especially suited to modeling amorphous alloys and glassy materials, for which traditional melt-quench strategies often fail to capture experimentally observed metastable states. The procedure is implemented through three interrelated stages, each meticulously designed to disrupt long-range crystallinity while preserving local atomic arrangements typical of non-crystalline solids.

1. Selection of a Structurally Unstable Crystalline Precursor

The initial phase involves selecting a crystalline structure exhibiting intrinsic instability—such as high-energy polymorphs, strained lattice configurations, or compositionally disordered alloys. This inherent structural instability facilitates disorder formation during subsequent thermal treatments by lowering the energy barriers associated with amorphization. For example, in Cu-Zr alloys, the selection of a precursor containing partial chemical disorder, such as Zr atoms occupying Cu lattice positions, effectively mirrors the structural frustration characteristic of amorphous alloys. Crucially, a thermodynamically stable crystalline configuration would inherently resist disordering and favor recrystallization during rapid cooling.

To ensure physical validity, the system density is constrained to align with experimental values of the corresponding amorphous phase (e.g., 6.2 g/cm³ for Cu₆₄Zr₃₆ [5]). In the absence of experimental density data, densities from crystalline analogs serve as practical approximations, although these may introduce subtle biases in atomic packing and thus necessitate post-validation analyses.

2. The ab initio Molecular Dynamics (AIMD) simulation process involves two dynamically distinct phases:

- **Heating (Disordering Phase):**
The system is gradually heated from 300 K to slightly below its equilibrium melting point (e.g., 1500 K in the Cu-Zr system). This sub-melting temperature is deliberately selected to maintain medium-range order while providing sufficient thermal energy to disrupt residual crystalline symmetry. During the initial 100 simulation steps (approximately 0.5–1.0 ps, depending on timestep size), atomic vibrations and bond disruptions occur, systematically destabilizing the lattice. This careful choice of temperature significantly mitigates the risk of crystalline domain nucleation, a prevalent issue in traditional melt-quench simulations.
- **Quenching (Kinetic Trapping):**
Subsequently, the system undergoes rapid cooling from the sub-melting temperature (1500 K) to 0 K over roughly 200 steps (~1–2 ps). This ultrafast quenching rate (~10¹³–10¹⁴ K/s) emulates kinetic arrest mechanisms found experimentally in methods such as splat cooling. The rapid temperature reduction effectively locks atoms into local minima of the potential energy landscape, stabilizing disordered configurations. Notably, characteristic asymmetric second peaks observed in Pair Distribution Functions (PDFs) typically result from this stage, highlighting the interplay between residual thermal disorder and emergent medium-range structural features.

3. Geometry Optimization (GO): Energy Minimization

Following the quenching phase, the structure undergoes geometry optimization through gradient-based energy minimization to eliminate unphysically high-energy atomic configurations, such as overlapping atoms or overstretched bonds that may arise from finite simulation timesteps in AIMD. Typically spanning approximately 1000 optimization iterations, this procedure systematically adjusts atomic positions to achieve interatomic forces below 0.01 eV/Å, thus refining local atomic coordination and ensuring adherence to fundamental quantum mechanical criteria while maintaining the amorphous nature induced during quenching.

Advantages over conventional melt-quench methods

The *undermelt-quench* approach effectively addresses two major shortcomings inherent to conventional melt-quench simulations:

- **Avoidance of Recrystallization Artifacts:** By maintaining sub-melting heating temperatures, this method prevents homogeneous crystalline nucleation, which frequently occurs during slow cooling from fully molten states.
- **Enhanced Computational Efficiency:** The significantly reduced heating and quenching durations (approximately 300 AIMD steps compared to several thousand steps in traditional methods) notably decrease computational demands without sacrificing the accuracy and fidelity of the resulting amorphous structures.

Connection to Experimental Observables

The *undermelt-quench* protocol faithfully reproduces experimentally observed PDF characteristics, such as split first peaks indicative of bond-length disorder, and asymmetric second peaks reflecting variations in medium-range atomic packing. For instance, in amorphous Pd [3], simulated PDF features such as second-peak asymmetry closely align with synchrotron X-ray experimental data, underscoring the method's robust capacity to capture intricate structural motifs, including distorted icosahedral configurations.

RESULTS AND DISCUSSION

Semiconductors

Amorphous Carbon

The pair distribution function (PDF) analysis of amorphous carbon (a-C) reveals insights into its local atomic arrangements, which are predominantly influenced by the hybridization states of carbon atoms. The first prominent peak in the PDF is typically observed around 1.56 Å (**Figure 1 (a)**), corresponding to the average C–C bond length in sp^3 -hybridized configurations, akin to those found in diamond-like structures. The presence of sp^3 -hybridized carbon atoms, indicates the presence of tetrahedral bonding environments.

Beyond the first coordination shell, the PDF distinctly exhibits a pronounced minimum (zero crossing) at 1.91 Å, indicative of a clear separation between first and second neighbor shells. Following this, a diminished and significantly broadened second coordination shell is observed within the range of approximately 2.0 Å to 3.0 Å, peaking clearly at 2.55 Å. This broadened feature reflects the increased variability in bond lengths and angles characteristic of amorphous structures, highlighting a substantial disorder beyond immediate atomic neighbors and suggesting diverse local structural configurations inherent to amorphous carbon.

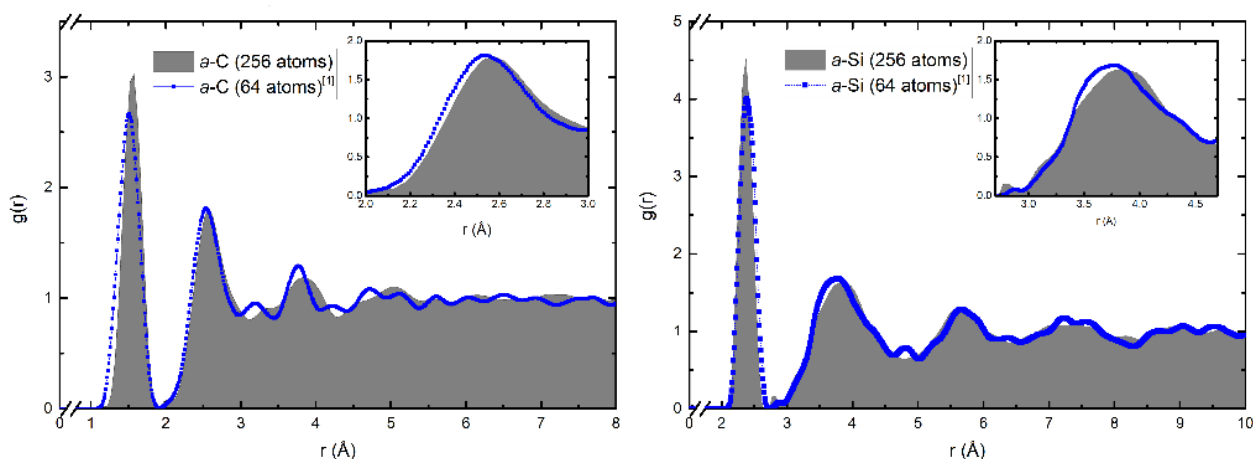


Figure 1. Comparison of the PDFs for a 256-atom supercell (Grey) and the 64-atom supercell (Blue dots) previously reported [1], for amorphous carbon (left) and amorphous silicon (right).

Amorphous Silicon

In amorphous silicon (a-Si), the PDF serves as a crucial tool for elucidating its disordered tetrahedral network. The first significant peak appears near 2.56 Å (**Figure 1 (b)**), corresponding to the average Si–Si bond length, slightly elongated compared to crystalline silicon due to the presence of bond angle distortions and coordination defects. The coordination number derived from this peak typically approximates four, consistent with the tetrahedral bonding motif, albeit with deviations arising from dangling bonds and undercoordinated sites.

After the first coordination shell, the PDF distinctly exhibits a near zero minimum at approximately 2.67 Å, indicating a clear separation between first and second neighbor shells. Subsequently, a diminished and significantly broadened second coordination shell is evident within the range of approximately 3.0 Å to 4.5 Å, with a clear peak at around 3.78 Å. This broadening reflects increased variability in bond lengths and angles typical of amorphous structures, signifying considerable structural disorder beyond immediate atomic neighbors and implying diverse local atomic arrangements intrinsic to amorphous silicon.

Subsequent peaks in the PDF of a-Si are less pronounced and broader, indicative of the absence of medium- and long-range order. Notably, subtle oscillations extending up to 20 Å have been reported, suggesting the presence of extended-range order beyond the first and second coordination shells. These features are attributed to the propagation of radial ordering from the first few atomic shells, contributing to the medium-range structural correlations observed in a-Si.

Metals

From **Figure 2** we can clearly identify a first peak that is notably narrow and pronounced, characteristic of well-defined short-range atomic order. However, in sharp contrast to semiconductors, the PDF does not approach zero between the first two peaks, indicating a continuous, albeit weaker, presence of structural correlations at intermediate distances. The second peak, depicted clearly in the inset, demonstrates a distinctive bimodal shape, emerging as a prominent and consistent feature in amorphous metallic systems.

This bimodal distribution, indicative of significant variations in local coordination and medium-range order, has been universally observed across all amorphous metals studied to date. Given its consistent presence and distinctive visual form resembling an elephant hidden beneath a sheet, we have aptly termed this feature the “elephant peak,” paying homage to the imaginative representation famously depicted in Antoine de Saint-Exupéry’s beloved children’s story, “Le Petit Prince” [9].

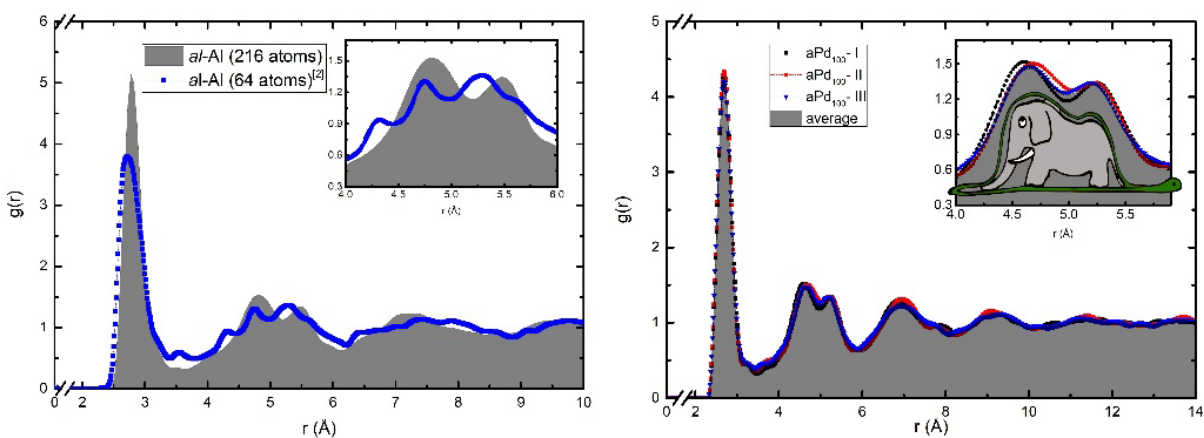


Figure 2. Comparison of the PDFs for a 216-atoms and the 64-atom for amorphous aluminum previously reported [2] (left). Predicted PDFs for three calculations of amorphous palladium with 216 atoms in the supercell [3]. Notice the elephant peak displayed in the inset.

A notable feature in **Figure 2** is the persistent non-zero valley observed between the first and second peaks. In certain instances, secondary peaks clearly emerge near the valley's minimum, highlighting the significant presence of atoms residing between traditional first and second neighbor shells. This phenomenon is critical, as it directly results from the structural rearrangements characteristic of the amorphization process. A possible explanation was proposed by Santiago *et al.* [10]. They propose that when atoms are displaced from their equilibrium lattice sites, they tend to reposition and occupy previously vacant spaces, thus stabilizing intermediate structural environments. These intermediate atomic positions, crucial for understanding the complex structural landscape of amorphous metals, are explicitly illustrated in **Figure 3**, underscoring their essential role in defining the local atomic configurations unique to amorphous systems.

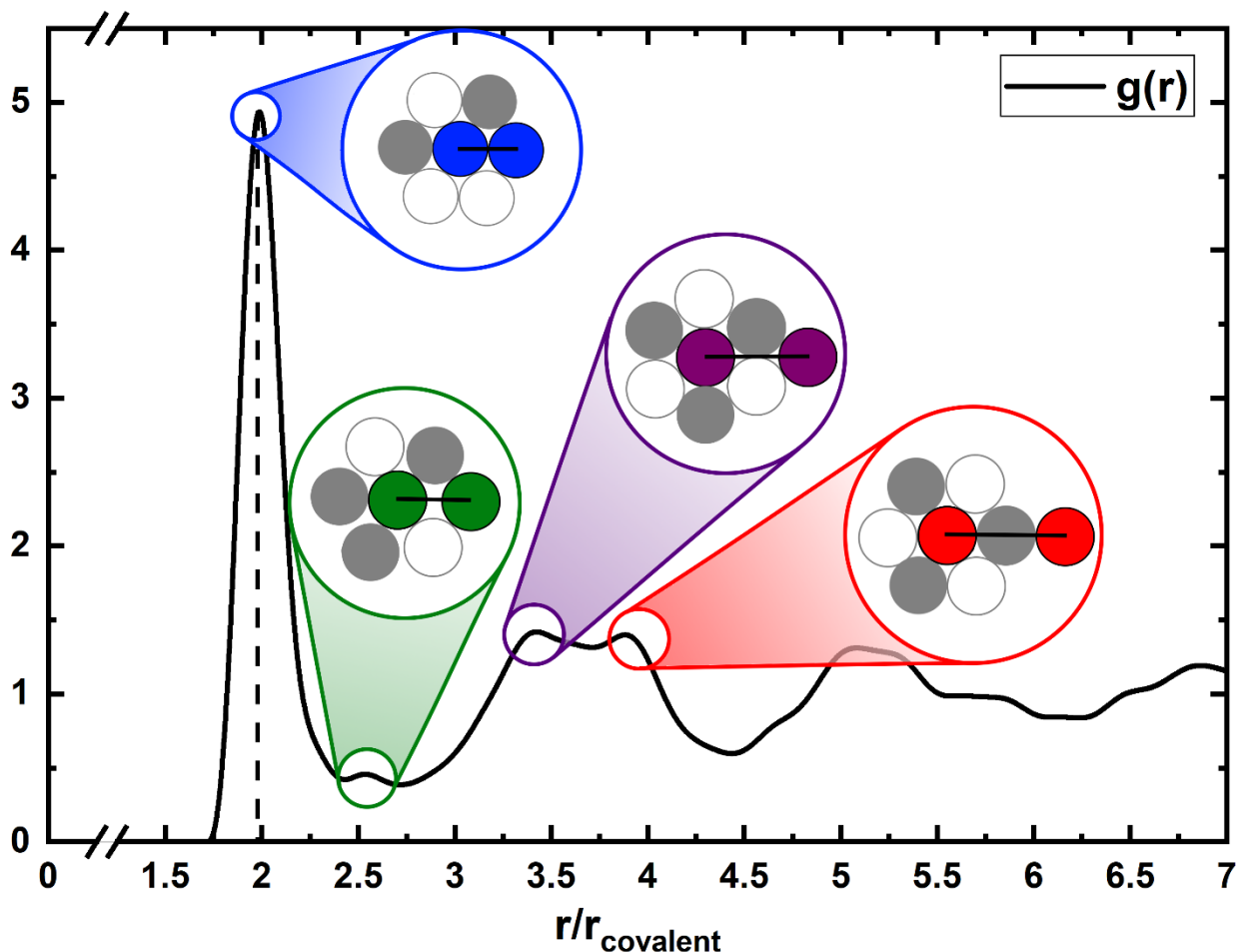


Figure 3. Schematic representation of four distinct types of local atomic clusters observed in an amorphous metallic system. Panel (a) illustrates atoms within the first neighbor shell, while panels (b) and (c) depict atoms occupying intermediate positions between the first and second neighbor shells—key sites that emerge due to structural rearrangements during the amorphization process. Panel (d) shows the configuration corresponding to the second neighbor shell. These cluster types are qualitatively illustrated in the adjacent figure and are discussed in detail in Reference [10].

Semimetals

As we move down the p-block of the periodic table, the band gap of elements progressively narrows, ultimately approaching zero. This trend marks the transition from classic semiconductors, such as carbon, silicon, and germanium, to semimetals like bismuth, and eventually to metals like lead. This continuous reduction in band gap is accompanied by significant changes in the atomic structure and bonding environment, which are captured effectively through the pair distribution function (PDF).

Amorphous Germanium

Figure 4 (a) highlights the unique structural position of germanium among these materials. It exhibits features common to both semiconductors and semimetals, functioning as a structural hybrid. The PDF of amorphous germanium shows a tall and narrow first peak—indicative of strong short-range order—followed by a deep but non-zero valley. This residual density between the peaks suggests the presence of atoms occupying intermediate regions, a characteristic beginning to emerge in materials undergoing a transition from covalent to more metallic bonding. Moreover, a nascent bimodal shape in the second peak is observed, reflecting early signs of the medium-range disorder typical of amorphous metals.

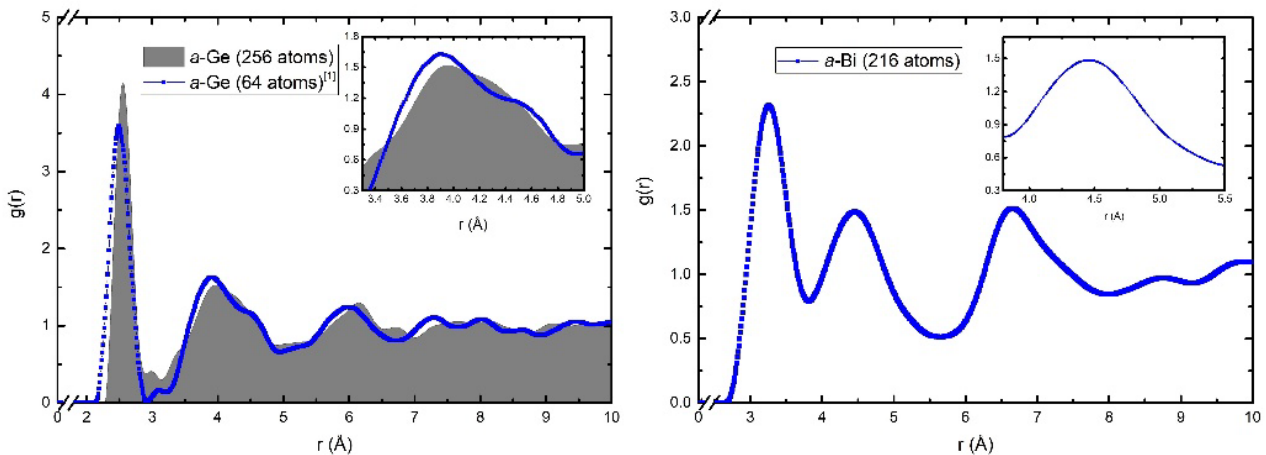


Figure 4. Comparison of the PDFs for a 256-atoms germanium supercell and the previously reported 64-atom supercell [1] (left). PDF for a 216-atoms supercell of amorphous bismuth previously reported [4] (right). Alloys and beyond

Amorphous Bismuth

Bismuth, a prototypical semimetal, presents a more complex structural picture. The first peak in its PDF is relatively tall and narrow but lacks the sharp definition found in pure metals. Importantly, the PDF does not drop to zero between the first and second peaks, signifying a continuous atomic distribution and substantial overlap between coordination shells. This makes precise determination of coordination numbers challenging, as discussed in Reference [4]. The second peak, illustrated in the insets of Figure 4, is unimodal, broader, and less intense than in crystalline or metallic phases—more akin to the profiles observed for semiconductors such as silicon and carbon. This behavior reinforces the notion that semimetals represent a structurally intermediate class, bridging the gap between disordered covalent networks and more densely packed metallic glasses.

Amorphous Alloys

The incorporation of multiple chemical elements into an alloy significantly increases the structural complexity of the resulting amorphous system, as evidenced in the pair distribution functions (PDFs) shown in Figure 5 for representative systems such as Cu-Zr and Au-Ag. In such alloys, the total PDF comprises a weighted sum of partial PDFs corresponding to each atomic pair type (e.g., Cu-Cu, Cu-Zr, Zr-Zr). This compositional diversity introduces intricate features, especially when the constituent elements have distinct atomic radii, bonding preferences, or electronic structures. The first peak in the total PDF is often the result of overlapping contributions from several partial PDFs, and similar superpositions occur for subsequent peaks. Consequently, the total PDF may exhibit bimodal or even multimodal features that are not attributable to a single atomic pair, but rather to the interference between overlapping local environments.

This emergent multimodality adds a considerable challenge to the interpretation of experimental PDFs. Often, it becomes exceedingly difficult to assign specific structural motifs to individual peaks, particularly in

disordered systems where partial PDFs cannot be directly measured. Nevertheless, a detailed inspection of the computed partial PDFs—such as those presented in Figure 5—reveals structural features consistent with those previously described for pure metals. For instance, the Cu–Cu partial in the Cu–Zr alloy displays a sharp and narrow first peak, followed by a pronounced non-zero valley and a bimodal second peak, characteristic of metallic bonding in amorphous phases. Similar trends are observed for the Cu–Zr and Zr–Zr partials, reinforcing the general picture of short-range order and medium-range disorder typical of metallic glasses.

In contrast, the Au–Ag alloy represents a limiting case where the chemical and structural similarity between the constituent elements leads to minimal structural differentiation in the partial PDFs. As a result, the total PDF closely resembles each of its partial components, exhibiting no signs of multimodality beyond the characteristic bimodal second peak—the so-called “elephant peak.” This highlights the role of chemical contrast in shaping the structural complexity of amorphous alloys and underscores the importance of analyzing partial PDFs to understand the interplay between local environments in multicomponent systems.

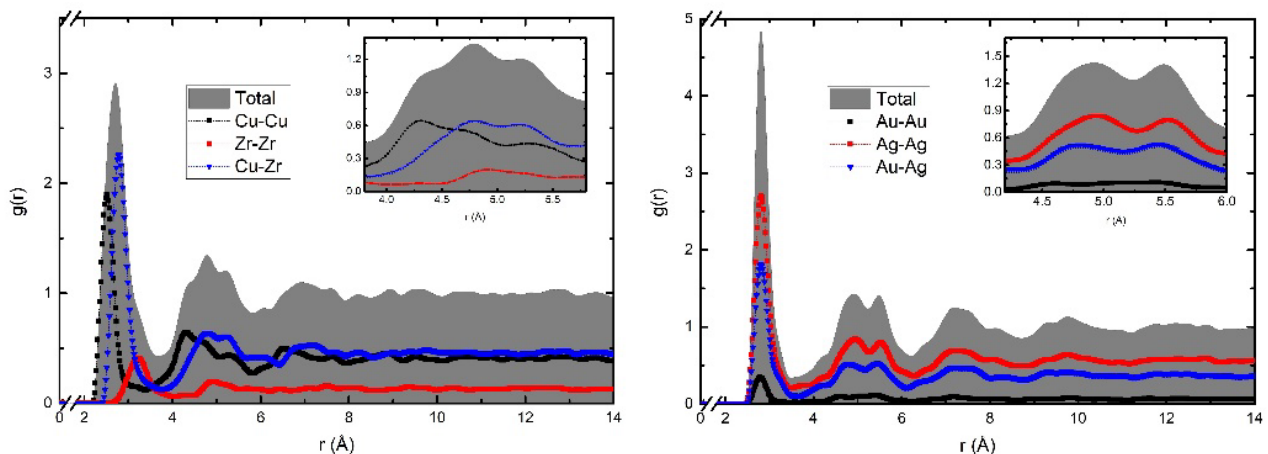


Figure 5. Comparison of the total PDF (Gray) with the partial-PDFs (colored marks) for amorphous Cu₆₄-Zr₃₆ alloy (left) and amorphous Au₂₅-Ag₇₅ alloy (right) with a 216-atoms supercell.

Liquids

FALTA hablar de líquidos.

FALTA FIGURA 6 de líquidos

FALTA agregar las aleaciones de Oscar, Gerardo, Alejandro y Edgar.

CONCLUSIONS

We report computationally generated amorphous materials for semiconductors, semimetals and metallic materials using the undermelt-quench approach developed in our group. The study of the pair distribution functions has proven an accurate tool for classifying different types of materials according to their structures and therefore their properties. There clearly are commonalities among the same class of materials and non-commonalities for different classes of materials, to the point that one has to wonder if it could be possible to describe a given class of materials in an integrated and unique fashion.

With this in mind, we propose that the pair distribution functions are a fundamental part of the study of amorphous materials. Pair distribution functions should be studied in detail to better understand the topological structure of non-crystalline solids and therefore their physical and chemical properties. Commonalities and non-commonalities should be carefully explored to identify trends and similarities.

ACKNOWLEDGMENTS

REFERENCES

- [1] F. Álvarez, C. C. Díaz, A. A. Valladares, *Phys. Rev. B*, 65, 113108 (2002).
- [2] A. A. Valladares, *J. Non-Cryst. Solids*, 353, 3540-3544 (2007).
- [3] I. Rodríguez, D. Hinojosa-Romero, R. M. Valladares, A. Valladares, A. A. Valladares, *Emergence of magnetism in amorphous palladium*, 2018 (unpublished).
- [4] Z. Mata-Pinzón, A. A. Valladares, R. M. Valladares, A. Valladares, *PLOS ONE*, 11(1): e0147645 (2016).
- [5] J. Galván-Colín, A. A. Valladares, R. M. Valladares, A. Valladares, *Physica B* 475, 140-147 (2015)
- [6] D. Hinojosa-Romero. MSc. Thesis, Universidad Nacional Autónoma de México (2018).
- [7] A. A. Valladares, J. A. Díaz-Celaya, J. Galván-Colín, L. M. Mejía-Mendoza, J. A. Reyes-Retana, R. M. Valladares, A. Valladares, F. Alvarez-Ramirez, D. Qu and J. Shen, *Materials*, 4, 716-781 (2011).
- [8] Dassault Systèmes BIOVIA, DMol3, CASTEP, Forcite, 2025, San Diego: Dassault Systèmes (2018).
- [9] A. de Saint-Exupéry, *Le Petit Prince*, (Reynal & Hitchcock, Paris, 1943) pp 1-2.
- [10] C. U. Santiago-Cortés, PhD. Thesis, Universidad Nacional Autónoma de México (2011).